RESEARCH ARTICLE

NANO · MICRO small
www.small-journal.com

Amorphous K–Co–Mo–S_x Chalcogel: A Synergy of Surface Sorption and Ion-Exchange

*Jing Nie, Taohedul Islam, Subrata Chandra Roy, Dien Li, Ruhul Amin, Kathryn Taylor-Pashow, Xianchun Zhu, Renfei Feng, Roman Chernikov, Avijit Pramanik, Fengxiang X. Han, Amar S. Kumbhar, and Saiful M. Islam**

Chalcogel represents a unique class of meso- to macroporous nanomaterials that offer applications in energy and environmental pursuits. Here, the synthesis of an ion-exchangeable amorphous chalcogel using a nominal composition of $K_2CoMo_2S_{10}$ (KCMS) at room temperature is reported. Synchrotron X-ray pair distribution function (PDF), X-ray absorption near-edge structure (XANES), and extended X-ray absorption fine structure (EXAFS) reveal a plausible local structure of KCMS gel consisting of $Mo^{5+}{}_2$ and $Mo^{4+}{}_3$ clusters in the vicinity of di/polysulfides which are covalently linked by Co^{2+} ions. The ionically bound K^+ ions remain in the percolating pores of the Co–Mo–S covalent network. XANES of Co K-edge shows multiple electronic transitions, including quadrupole (1s→3d), shakedown (1s→4p + MLCT), and dipole allowed 1s→4p transitions. Remarkably, despite a lack of regular channels as in some crystalline solids, the amorphous KCMS gel shows ion-exchange properties with $UO_2{}^{2+}$ ions. Additionally, it also presents surface sorption via [S••••$UO_2{}^{2+}$] covalent interactions. Overall, this study underscores the synthesis of quaternary chalcogels incorporating alkali metals and their potential to advance separation science for cations and oxo-cationic species by integrating a synergy of surface sorption and ion-exchange.

1. Introduction

Chalcogel is an emerging class of chalcogenide-based aerogel that consists of highly disordered nanoaggregated particles of chalcogenide clusters.[1–3] This class of materials possesses high internal surface area, ultra-low density, and meso- to microporosities besides their various intriguing chemical properties, including surface polarizability and semiconductivity.[1] An integration of such diverse physicochemical properties makes chalcogels appealing for a large variety of applications, including photocatalyst,[4,5] solar fuels,[4,6] electrocatalysis,[7] adsorption, environmental remediation,[8–13] and electrochemical energy storage and conversion.[14]

In general, chalcogels consist of monomeric units of (metal-) chalcogenides which are interlinked either by chalcogen-chalcogen or by metal-chalcogenide covalent bonding interactions.[6,15,16] This kind of building features lead to the condensation of the monomeric chalcogenide clusters into covalently bonded networks extending into three dimensions in space. Since the discovery of chalcogenides-based aerogels in the early 2000s,[1,3] this class of materials has been investigated because of their appealing chemistry of chalcogen-chalcogen bonds that results in the formation of chalcogenide-based backbone with Lewis basic and polarizable characters.[4,7,12,17,18]

J. Nie, T. Islam, S. C. Roy, A. Pramanik, F. X. Han, S. M. Islam
Department of Chemistry, Physics, and Atmospheric Sciences
Jackson State University
Jackson, MS 39217, USA
E-mail: muhammad.s.islam@jsums.edu

D. Li, K. Taylor-Pashow
Savannah River National Laboratory
Aiken, SC 29808, USA

R. Amin
Electrification & Energy Infrastructure Division
Oak Ridge National Laboratory
Oak Ridge, TN 37831, USA

X. Zhu
Department of Civil Engineering
Jackson State University
Jackson, MS 39217, USA

R. Feng, R. Chernikov
Canadian Light Source
Saskatoon, Saskatchewan S7N2V3, Canada

A. S. Kumbhar
Chapel Hill Analytical and Nanofabrication Laboratory (CHANL) &,
Department of Chemistry
University of North Carolina at Chapel Hill
Chapel Hill, NC 27599, USA

The ORCID identification number(s) for the author(s) of this article can be found under https://doi.org/10.1002/smll.202400679

DOI: 10.1002/smll.202400679

Chalcogels can be synthesized by a variety of solution-processable synthetic routes, such as thiolysis, nanoparticle condensations, metathesis synthesis, oxidative coupling, polymeric condensations, and hydrolysis.[9,19,20] Among these, the metathesis synthesis route, developed by Kanatzidis and Coworkers,[21] involves the coordinative reactions of chalcogenide anions with metal cations to form a covalent network of the chalcogel. This synthetic route has yielded a large variety of covalently bonded chalcogels with diverse anionic building blocks of chalcogens, such as $[MQ_4]^{4-}$, $[M_2Q_6]^{4-}$, and $[M_4Q_{10}]^{4-}$ (M = Ge, Sn; Q = S, Se),[1,11] $[MQ_4]^{2-}$ (M = Mo, Q = S, Se), $[Mo_3S_{13}]^{2-}$, $[MQ_3]^{3-}$ (M = Sb, As; Q = S, Se),[1,2,11,18,22] and polysulfide ligands, S_n^{2-} (n = 3, 4, and 5).[17,23] Transition and/or p-block metal cations serve as linkers for these chalcogenide building blocks, resulting in covalent networks of metal-(poly)sulfide chalcogels that extend across all dimensions of space.[24]

In contrast to the vast chemistry of amorphous chalcogels with only covalent bonding features, their chemistry with electrostatically bound cations is scarce.[10,17,25] Hence, incorporating alkali metals into the covalent networks of metal chalcogenides can introduce electrostatic bonding characteristics into the covalent network of transition metal sulfide chalcogels. These alkali metal ions could potentially be exchanged with various chemically soft metal cations or oxo-cationic species, including uranyl ions $[O = U^{6+} = O]^{2+}$. Besides, the introduction of alkali metals into the covalent matrix of the chalcogels can expand the chemistry of amorphous chalcogels to robust chemical compositions and versatile local structures, which in turn can unveil new properties.

Notably, the ion-exchange features of crystalline solids with open frameworks or layered structures are common, which is mainly due to the presence of electrostatically bound cations in the periodic covalent framework of the crystalline compound.[19,26,27] In contrast to crystalline materials, this feature is still fancy in amorphous solids, which may be due to the lack of periodic atomic arrangement. Moreover, the chalcogel nanoparticles consist of a high density of polysulfides and show potential for the binding of chemically soft Lewis acidic metal cations or cationic centers of oxoanions through surface sorption, following the Hard–Soft Lewis Acid–Base (HSAB) principle.[11,28,29] Thus, it is of utmost interest to explore the chemistry of chalcogels with alkali metal cations for novel chemical compositions, understand their local structures, elucidate their interactions with radioactive oxocations of UO_2^{2+}, and unveil the synergy of surface sorption and ion-exchange. These findings will not only enrich our understanding of the chemistry of chalcogels but also will play a vital role in determining the design principles to develop superior sorbents for chemically diverse metal cations.

Herein, we report the synthesis, local structures, electronic properties, and interactions of UO_2^{2+} for amorphous KCMS chalcogel. By synchrotron X-ray pair distribution function (PDF), X-ray absorption near edge structure (XANES), and extended X-ray absorption fine structure (EXAFS), we present the intricate local structures of KCMS, which plausibly consist of diverse coordination polyhedra of Co^{2+} and $Mo^{4+,5+}$ in the vicinity of (poly)sulfides. Within this arrangement, the K^+ ions are integrated into the covalent network of Co–Mo–S. We also show that amorphous KCMS gel exhibits both surface sorption and ion-exchange characters for $[O = U = O]^{2+}$ cation. This finding offers a promising paradigm to develop quaternary chalcogels with alkali metals, potentially contributing to the field of separation science for removing inorganic cationic species from water.

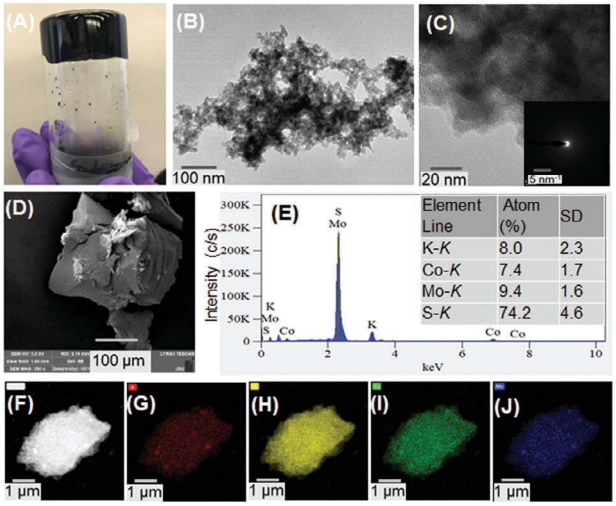

Figure 1. Photograph of the inverted vial showing the strength of the monolith KCMS wet–gels against fragmentation A), TEM image of the aerogels demonstrates the aggregation of the nanoparticles along with diverse range of porosities B), HRTEM image and the SAED image, in the inset of C) showing no evidence of the crystallites formation, SEM image D), and EDS spectrum E) showing bulk scale morphology and chemical compositions, STEM-HAADF elemental mapping showing the distribution for K, S, Co, and Mo in the porous KCMS F–J) aerogel.

2. Results and Discussion

Spongy monolith wet–gel of the novel K–Co–Mo–S_x (KCMS) was synthesized by metathesis route in solution with a nominal composition of $K_2CoMo_2S_{10}$ (**Figure 1A**). The gelation occurs by covalent interactions of Co, Mo, and S that result in the formation of a 3D extended porous network, and K^+ ions remain in the pores of the covalent networks of Co–Mo–S through electrostatic interactions. The wet–gel of KCMS was fabricated to aerogels by the exchange of gels' pore-filled liquid ethanol with CO_2 using supercritical drying, while the xerogel was obtained by drying at ambient conditions. The 3D cross-linked colloidal matrix of the aerogels was resilient against breaking into pieces during regular handling in the laboratory. High-resolution transmission electron microscopy (HRTEM) and scanning transmission electron microscopy (STEM) investigations reveal the porous characteristics of aggregated colloidal nanoparticles in the KCMS aerogel, exhibiting irregular sizes and shapes (Figure 1B). The interconnected nanoparticles of the KCMS gels are assembled in space with a high density of randomly arranged meso- (2–50 nm) and macro- (≥ 50 nm) porosities (Figure 1B). We see additional evidence of porous features by surface area measurements. We prepared multiple batches of aerogels that resulted in a maximum BET surface area of about 90 $m^2\ g^{-1}$, with an average surface area of 67.0 ± 16.4 $m^2\ g^{-1}$, and average pore diameters of 34.3 ± 5 nm for adsorption and 40.3 ± 7 nm for desorption (Figure S1, Supporting Information). Besides, HRTEM

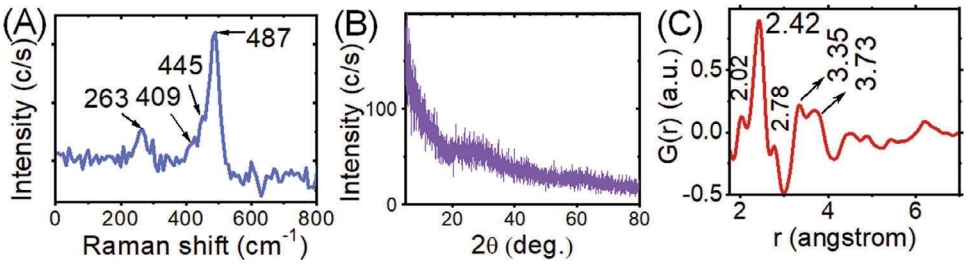

Figure 2. A) Raman spectrum of the KCMS showing the presence of S_n^{2-} group; B) XRD demonstrates a highly disordered amorphous feature; C) PDF shows the local ordering of the atoms, including Mo—Mo and S—S interactions, in the KCMS gels.

shows no evidence of the presence of any crystalline phase, indicating the amorphous nature of the KCMS gel (Figure 1C). Selected area electron diffraction (SAED) displays diffused rings, further confirming its amorphicity (Figure 1C inset). Scanning electron microscopy (SEM) image of the aerogels shows the morphological homogeneity and fluffy nature of the KCMS chalcogel (Figure 1D). SEM/EDS analysis of the K–Co–Mo–S chalcogel, synthesized from various batches were collected in micrometer length scales, indicated an average atomic abundance of K, Co, Mo, and S as 8.0 ± 2.3, 7.4 ± 1.7, 9.4 ± 1.6, and 74.2 ± 4.6%, respectively (Figure 1E). In contrast, TEM/EDS data were collected in nanometer length scales of the KCMS gels, and the analysis of the data revealed an average abundance of 6.3 ± 2.1, 4.0 ± 0.5, 10.4 ± 0.7, and 79.4 ± 2.7% for K, Co, Mo, and S, respectively (Figure S2, Supporting Information). Thus, the compositional ratios of the elements in the different chalcogels obtained by SEM/EDS and TEM/EDS remain in close proximity within the limits of the standard deviation. Besides, the high-angle annular dark-field (HAADF)-STEM images further show the homogeneity of the gels, on a micron scale, with a uniform distribution of K, Co, Mo, and S atoms (Figure 1F–J). Furthermore, it is noteworthy that after synthesizing KCMS gels, we made efforts to synthesize analogous gels Na–Co–Mo–S_x (NaCMS, Figure S3, Supporting Information). The EDS analysis of these gels revealed negligible content of Na^+ in the covalent network of Co–Mo–S chalcogels. This could be because of the greater ionic characteristics of Na^+ compared with K^+ ions, although the exact reason remains unclear.

The Raman spectrum of the black KCMS gel shows a series of peaks at 263, 409, 445, and 487 cm^{-1} (**Figure 2**A). The strong peak at 487 cm^{-1} and the shoulder at ≈445 cm^{-1} can be attributed to the symmetric and antisymmetric vibration of the —S—S— bonds demonstrating the presence of polysulfide species, (S_n^{2-}) in the structure of the KCMS.[30] Besides, the peaks at about 409 and 263 cm^{-1} may be representative of Mo/Co–S and K–S vibrational energy, respectively. X-ray powder diffraction (XRD) of the KCMS is featureless, except for a weak hump in the range of 2θ ≈20° to 30° suggesting the absence of long-range ordering of the atomic arrangement (Figure 2B). Synchrotron X-ray pair distribution function (PDF) analysis shows an atomic correlation up to ≈6 Å (Figure 2C), which represents the absence of a long-range translational symmetry of the KCMS gels, as we observed by XRD.

The PDF analysis of the KCMS chalcogel revealed a prominent peak at 2.42 Å, indicative of the presence of Mo—S bonding correlation, aligning with the Mo—S interatomic distance observed in the Mo_3S_{13} anions of the crystalline $(NH_4)_2Mo_3S_{13}$.[31,32] The PDF of the KCMS revealed an atomistic correlation with a peak centered at ≈2.0 Å, which is consistent with the S—S bonding correlation of the S_n^{2-} (n ≥ 2) group. Moreover, PDF shows a peak at 2.78 Å, which corresponds to the Mo—Mo correlation.[2,33] The evidence of S—S and Mo—Mo bonding correlation is indicative of the presence of a bi- or trinuclear cluster of molybdenum (Mo_2 and Mo_3), as related to the crystalline molecules of $(NH_4)_2Mo_2(S_2)_6$ or $(NH_4)_2Mo_3S(S_2)_6$.[31,32,34] Moreover, an intense band at about 3.3 Å may related to the S····S correlation for the first coordination polyhedra of the Mo/Co—S.[2] Besides, the peak at 3.7 Å can be attributed to the superimposed correlations of K····S and M····M (M = Mo and Co), respectively.

To evaluate the electronic structure, we investigated KCMS gels by X-ray photoelectron spectroscopy (XPS) and X-ray absorption near-edge structure (XANES), (**Figure 3**; Figure S4, Supporting Information). XPS reveals peaks at ≈779.4 and 782.0 eV (Figure 3A), which reflect binding energy (BE) of the Co 2p orbitals and its related satellite peak, respectively. This value of BE may represent the Co^{2+} oxidation state in the vicinity of the sulfide ligand.[35] Mo $3d_{5/2}$ and $3d_{3/2}$ orbital excitation energy appeared in the range of 228.7 to 231.8 eV, respectively (Figure 3B), consistent with the Mo^{4+} oxidation state.[32,26,20] Besides, the extended tailing of the 231.8 (Mo^{4+} $3d_{3/2}$) eV peak close to ≈234 eV and the relative higher intensity of Mo^{4+} $3d_{3/2}$ peak as compared to its $3d_{5/2}$ can be attributed to the superimposition of Mo^{4+} $3d_{3/2}$ and Mo^{5+} $3d_{5/2}$. XPS revealed bands centered at ≈292.1 and

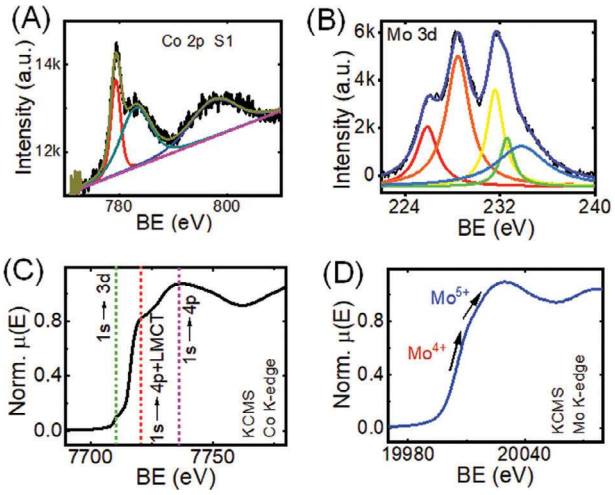

Figure 3. X-ray photoelectron spectra of Co A), and Mo B); the XANES spectra of C) Co K-edge, and D) Mo K-edge of the K–Co–Mo–S gel.

294.8 eV, which are characteristics of the $2p_{3/2}$ and $2p_{1/2}$ energies of K^+ cations (Figure S4A, Supporting Information).[36] Furthermore, the peaks at 162.6 and 168.6 eV (Figure S4B, Supporting Information) are consistent with the S 2p orbital excitation energy.[34,37] Indeed, the deconvoluted peaks at 162.6 eV originated from the sulfur 2p of polysulfide species, while the broad peak centered at 168.6 eV is attributed to the oxidation of the surface sulfides of KCMS nanoparticles because of their prolonged exposure to air.[26,38] This feature is commonly observed for other chalcogels' nanoparticles.[9]

Co K-edge XANES of the KCMS chalcogel (Figure 3C) features three significant regions or peaks demonstrating the electronic transitions in the photon absorbing atom "Co". The weak pre-edge peak ≈7710 eV results from the dipole forbidden quadrupole 1s→3d bound state transition, a common characteristic of the K-edge of first-row transition metals having open 3d orbitals, and this happens due to the mixing of ligand 4p and metal 3d orbitals.[29,39] Besides, the shoulder at ≈7720 eV along the rising edge likely represents the shakedown transition that consists of a simultaneous 1s→4p and ligand (sulfur) 3p to Co 3d charge transfer transitions (LMCT).[40] The "shakedown-transition" occurs because the metal 3d orbital has lower energy than its ligand's 3p orbital, which is due to the creation of a hole at the core shell that allows the nucleus to pull down the 3d orbital.[40] The simultaneous 1s→4p + LMCT comes at lower energy than the actual 1s→4p transition which is the third peak or the edge maxima of the XAS spectra that we observe at ≈7736 eV. For the Mo K-edge, the XANES doesn't have any pre-edge peak but the rising edge of the XAS spectra has a small change in slope, which presumably is because of the mixed valance state of the Mo centers (4+ and 5+) present in the system (Figure 3D). We also observed the mixed valency of Mo by XPS, as discussed above. The dipole-forbidden transitions for the K-edge of the 4d transition metals are not always very distinctive since these transitions happen at higher energy and the very short core-hole lifetime governs the line width.[29]

EXAFS analysis of the KCMS gel was carried out using a Python-based "Larch" software package for both the Mo and Co K-edge spectra (**Figure 4**).[41] The EXAFS equation (Equation 1) is used to calculate the EXAFS oscillation $\chi(k)$ and some other parameters that will contribute to the construction of the model.[42]

$$\chi(k) = \frac{N_j F_j(k) \exp\left[-\frac{2R_j}{\lambda(k)}\right]}{kR_j} \exp\left[i2kR_j + i\delta_j(k)\right] \quad (1)$$

The parameters that are of principal interest to analyze the coordination environment are the number of scattering atoms N_j, and the absorber-scatterer distance R_j, subscript j represents each of the scattering paths, k is EXAFS wavenumber, $\lambda(k)$ being the mean-free path, $F_j(k)$ is the effective scattering amplitude, $\delta(k)$ is the phase shift. To fit the Co K-edge EXAFS data, three different phases and six different feff paths were used, and the fitting parameters are listed in Tables S1 and S2 (Supporting Information). The Co—S path ≈2.25 Å obtained from CoS with the coordination number six suggests the presence of octahedral cobalt sulfide geometry in KCMS gel.[43] In the r space data, there is a tiny bump before the main peak (around 2 Å), which was fitted using a Co—S path around 1.89 Å with a coordination number

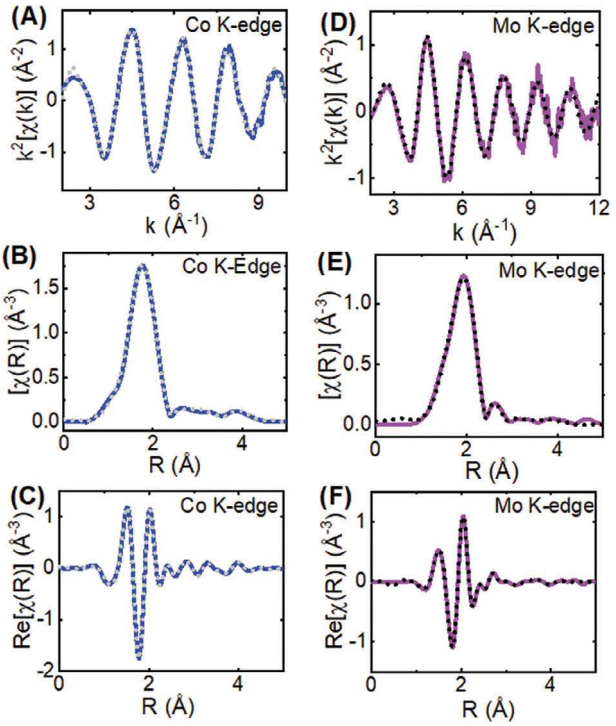

Figure 4. EXAFS spectra (solid line) with the fitted model (dash) of the pristine KCMS chalcogel: Co K-edge in A) k space, B) r space, and C) real space and of the Mo K-edge in D) k space, E) r space and F) real space.

of four from the reference compound Co_9S_8.[44] This path represents the four-fold geometry of Co—S polyhedra that should remain in the KCMS chalcogel. Besides, the damped peaks after the main peaks in the r space data reflect Co—Co scattering around 2.51 Å and Co—Mo bonding around 2.63 Å in the first coordination sphere. The reference compound for the Co—Mo path was $CoMo_2S_4$, and this path represents the gel network having Co ions as linkers of the Mo—S polyhedra.[45] Although the reference compounds that were used for the feff calculations do not reflect the exact local geometry of the KCMS, it suggests a probable local coordination geometry. The scattering path of Co—S around 4.64 Å indicates the intercluster scattering of the photoelectron. The overall R factor of the fitted model is 0.002, which is in the acceptable range with the χ^2 and reduced χ^2 values of 0.24 and 0.02, respectively.

The Mo K-edge data was fitted using both the $(NH_4)_2Mo_2S_{12}$ and $(NH_4)_2Mo_3S_{13}$, where they contain a bi- and tri-nuclear cluster of Mo in the vicinity of sulfides for their corresponding $Mo_2^{V}(S_2)_6$ and $Mo_3^{IV}S(S_6)_2$.[31,32] The coordination numbers during the fitting in both Mo and Co K-edge EXAFS were kept fixed to reduce the number of parameters. Two different Mo—S scattering paths: one around 2.39 Å with the coordination number six, and another around 2.08 Å with the coordination number five, and hence, the fit of the most intense peak in the r space data remains in statistical error limits. This finding suggests the presence of Mo—S coordination that resembles to $Mo_2^{V}(S_2)_6$ and $Mo_3^{IV}S(S_6)_2$, respectively. Besides, the second-most intense peak in the r space data of Mo K-edge was best fit with two different Mo—Mo paths, i) one at ≈2.5 Å with a coordination

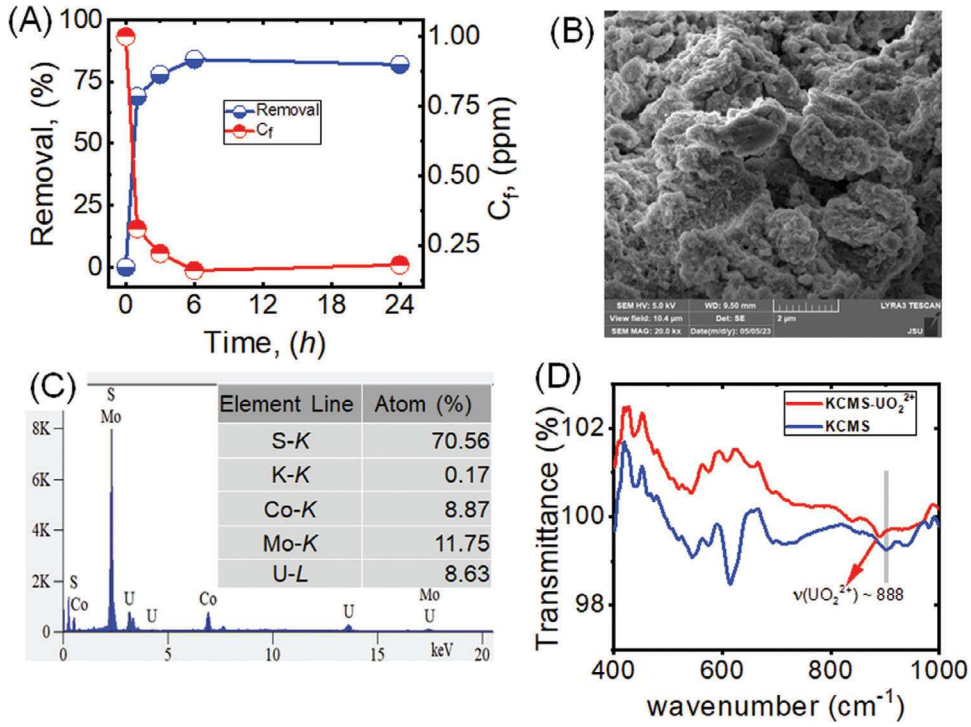

Figure 5. A) Time-dependent removal percentage and the final concentration of uranium after sorption by KCMS; B) SEM image of the spent KCMS; C) EDS of UO_2^{2+} interacted KCMS xerogel showing the presence of uranium and (nearly) absence of K^+ ion, suggesting exchange of K^+ ion by the linear $[O = U = O]^{2+}$, in inset showing the average atomic abundance for the post interacted KCMS; D) a comparison of IR spectra showing the appearance of the peak near 888 cm^{-1} at the UO_2^{2+} treated KCMS which corresponds to UO_2^{2+}.[51]

number 1.8 (close to 2), which was calculated using $(NH_4)_2Mo_2S_{12}$ as a model compound; ii) the other at ≈2.7 Å having a coordination number three which was calculated using $(NH_4)_2Mo_3S_{13}$ as a mode to fit the data. This shows the presence of both dinuclear and trinuclear molybdenum (Mo_2, Mo_3), as related to $Mo_2^{V}(S_2)_6$ and $Mo_3^{IV}S(S_6)_2$, in the KCMS gel. A similar local structure was observed for MoS_x-GO chalcocarbogels.[46] These clusters may be interconnected by Co ions which can be realized from the presence of a Co—Mo scattering path in the Co K-edge EXAFS (Table S1, Supporting Information). Deducing the local structures of the amorphous chalcogenide gels is an arduous task, especially for such a complex K–Co–Mo-S quaternary system. However, our modeling of the EXAFS with these reference compounds provides a plausible understanding of the local structures.

To understand the chemical interactions of KCMS with uranyl cations (UO_2^{2+}), we interacted this material with UO_2^{2+} cations at various time scales. A kinetic study reveals promising results, showing that xerogels of KCMS can efficiently remove ≈84% from 1000 ppb spiked solutions (**Figure 5A**; Table S3, Supporting Information) within 6 h. Additionally, the material exhibited interaction with 5 mmol solutions of uranium, leading to a uranium sorption capacity of 117.4 mg g^{-1}. Although this value of capacity is comparable to that of other materials, such as graphene aerogel (131 mg g^{-1}),[47] KTMS aerogels (167 mg g^{-1}),[25] MoS_2 nanosheet (45.7 mg g^{-1}),[48] MoS_2 nanoflowers (37.1 mg g^{-1}),[48] and SDS/MoS_2 (98.4 mg g^{-1}),[49] it is noteworthy that it possesses lower capacity compared to crystalline metal sulfide ion-exchangers, specifically $K_2MnSn_2S_6$ (380 mg g^{-1})[50] and $K_{2x}Sn_{4-x}S_{8-x}$ (287 mg g^{-1}).[36] This may be attributed to the lower molar concentration of K^+ in KCMS compared with crystalline $K_2MnSn_2S_6$ (380 mg g^{-1})[50] and $K_{2x}Sn_{4-x}S_{8-x}$[36] as well as the lack of periodicity in the amorphous structure. However, despite this difference, chalcogels offer advantages such as room-temperature and scalable synthesis, compositional diversity, porous nature, ion-exchange properties, and surface polarizable characteristics of their nanoparticles. Therefore, this finding highlights the importance of exploring new chalcogels with ion-exchange properties and unveil the synergy of sorption and ion-exchange phenomena.

Analysis of the post-interacting KCMS gels with UO_2^{2+} by EDS revealed the presence of 8.6 atomic percentage of uranium, however, it displayed nearly the absence of K^+ ions (Figure 5C). Hence, the presence of uranium and the absence of K^+ (nearly) indicates the exchange of K^+ by UO_2^{2+} ions. Here the diffusion of the UO_2^{2+} cations into the chalcogels may be facilitated by the formation of linear $[O = U = O]^{2+}$ ions, similar to the phenomena described for $K_2MnSn_2S_6$.[19,50] The linear geometry of the $[O = U = O]^{2+}$ oxo-cation facilitates its penetration into the percolating network of K–Co–Mo–S_x gels. The IR spectrum of the UO_2^{2+} interaction shows (Figure 5D) the presence of a peak at ≈888 cm^{-1}, which corresponds to $[O = U = O]^{2+}$ vibration energy.[51] Notably, for the complete exchange of monovalent K^+ ions by the divalent UO_2^{2+}, according to EDS, it needs about four atomic percent of UO_2^{2+}. Hence, a larger atomic abundance of the uranium (≈8.6%) can be attributed to the surface sorption by the KCMS gel particles through a $[O_2^{2+}U\cdots S—]$ covenant interactions following the Pearson's Hard Soft Acid Base principle

(HSAB).[28] This kind of surface sorption by KCMS chalcogels is reported previously by Kanatzidis and Co-workers.[52] Overall, our findings suggest KCMS attributes both ion-exchnage and surface sorption for the sorption of UO_2^{2+} ions.

3. Conclusion

This work demonstrates the stabilization of electrostatically bound K^+ ions in the covalent network of Co–Mo–S to produce K–Co–Mo–S chalcogel. The aerogel of KCMS is amorphous, but it contains structural features relevant to Mo_2 and Mo_3 clusters in the vicinity of sulfides that plausibly be related to crystalline molecular $Mo_2^{V}(S_2)_6$ and $Mo_3^{IV}S(S_6)_2$ anions. In contrast, Co-sites attain six and four coordinated Co—S polyhedra which connect the Mo—S anionic clusters. Co K-edge XANES revealed three different transitions: low energy dipole forbidden quadrupole transition, 1s→3d; shakedown transitions, 1s→3d + MLCT; and a dipole allowed transition,1s→4p. Additionally, KCMS gels exhibit surface sorption characteristic for UO_2^{2+} through a $[O_2^{2+}U\cdots S—]$ covenant interactions beside the exchange of K^+ with UO_2^{2+}. Overall, this work presents opportunities to synthesize complex multinary chalcogels with versatile chemical compositions in the systems of alkali metal — transition/p-block metal cations — metal chalcogenide anionic clusters, unfold the local structures of the amorphous chalcogels, and elucidate their properties relevant to the sorption of metal cations and oxocationic species.

Supporting Information

Supporting Information is available from the Wiley Online Library or from the author.

Acknowledgements

This work was supported by the US Department of Energy Minority Serving Institution Partnership Program (MSIPP) managed by the Savannah River National Laboratory under BSRA contract (RFP No. 0000542525 and 0000458357). SCR is thankful to the NSF Division of Chemistry (NSF-2100797). This research used resources from the Advanced Photon Source, a U.S. Department of Energy (DOE) Office of Science User Facility operated for the DOE Office of Science by Argonne National Laboratory under Contract No. DE-AC02-06CH11357. The mail-in program at Beamline 11-ID-B contributed to the data. X-ray absorption spectroscopy measurements were performed at the VESPERS and BioXAS beamlines, Canadian Light Source, which was supported by the Canada Foundation for Innovation (CFI), the Natural Sciences and Engineering Research Council (NSERC), the National Research Council (NRC), the Canadian Institutes of Health Research (CIHR), the Government of Saskatchewan, and the University of Saskatchewan. Any use of trade, firm, or product names is for descriptive purposes only and does not imply endorsement by the U.S. Government. TEM images were taken in part at the Chapel Hill Analytical and Nanofabrication Laboratory, CHANL, a member of the North Carolina Research Triangle Nanotechnology Network, RTNN, which was supported by the National Science Foundation, Grant ECCS-2025064, as part of the National Nanotechnology Coordinated Infrastructure, NNCI.

Conflict of Interest

The authors declare no conflict of interest.

Data Availability Statement

The data that support the findings of this study are available in the supplementary material of this article.

Keywords

aerogel, chalcogels, ion-exchange, quadrupole and shakedown transitions, UO_2^{2+} separation

Received: January 27, 2024
Revised: March 1, 2024
Published online:

[1] S. Bag, P. N. Trikalitis, P. J. Chupas, G. S. Armatas, M. G. Kanatzidis, *Science* **2007**, *317*, 490.
[2] S. Bag, A. F. Gaudette, M. E. Bussell, M. G. Kanatzidis, *Nature Chem* **2009**, *1*, 217.
[3] J. L. Mohanan, I. U. Arachchige, S. L. Brock, *Science* **2005**, *307*, 397.
[4] B. D. Yuhas, A. L. Smeigh, A. P. S. Samuel, Y. Shim, S. Bag, A. P. Douvalis, M. R. Wasielewski, M. G. Kanatzidis, *J. Am. Chem. Soc.* **2011**, *133*, 7252.
[5] Y. Shim, R. M. Young, A. P. Douvalis, S. M. Dyar, B. D. Yuhas, T. Bakas, M. R. Wasielewski, M. G. Kanatzidis, *J. Am. Chem. Soc.* **2014**, *136*, 13371.
[6] Y. Shim, B. D. Yuhas, S. M. Dyar, A. L. Smeigh, A. P. Douvalis, M. R. Wasielewski, M. G. Kanatzidis, *J. Am. Chem. Soc.* **2013**, *135*, 2330.
[7] B. D. Yuhas, C. Prasittichai, J. T. Hupp, M. G. Kanatzidis, *J. Am. Chem. Soc.* **2011**, *133*, 15854.
[8] I. R. Pala, S. L. Brock, *ACS Appl. Mater. Interfaces* **2012**, *4*, 2160.
[9] K. S. Subrahmanyam, C. D. Malliakas, S. M. Islam, D. Sarma, J. Wu, M. G. Kanatzidis, *Chem. Mater.* **2016**, *28*, 7744.
[10] K. S. Subrahmanyam, C. D. Malliakas, D. Sarma, G. S. Armatas, J. Wu, M. G. Kanatzidis, *J. Am. Chem. Soc.* **2015**, *137*, 13943.
[11] Y. Oh, S. Bag, C. D. Malliakas, M. G. Kanatzidis, *Chem. Mater.* **2011**, *23*, 2447.
[12] B. J. Riley, J. Chun, J. V. Ryan, J. Matyáš, X. S. Li, D. W. Matson, S. K. Sundaram, D. M. Strachan, J. D. Vienna, *RSC Adv.* **2011**, *1*, 1704.
[13] K. S. Subrahmanyam, I. Spanopoulos, J. Chun, B. J. Riley, P. K. Thallapally, P. N. Trikalitis, M. G. Kanatzidis, *ACS Appl. Mater. Interfaces* **2017**, *9*, 33389.
[14] V. V. T. Doan-Nguyen, K. S. Subrahmanyam, M. M. Butala, J. A. Gerbec, S. M. Islam, K. N. Kanipe, C. E. Wilson, M. Balasubramanian, K. M. Wiaderek, O. J. Borkiewicz, K. W. Chapman, P. J. Chupas, M. Moskovits, B. S. Dunn, M. G. Kanatzidis, R. Seshadri, *Chem. Mater.* **2016**, *28*, 8357.
[15] X. Shan, J. Liu, H. Mu, Y. Xiao, B. Mei, W. Liu, G. Lin, Z. Jiang, L. Wen, L. Jiang, *Angew. Chem., Int. Ed.* **2020**, *59*, 1659.
[16] S. Bag, I. U. Arachchige, M. G. Kanatzidis, *J. Mater. Chem.* **2008**, *18*, 3628.
[17] Y. Oh, C. D. Morris, M. G. Kanatzidis, *J. Am. Chem. Soc.* **2012**, *134*, 14604.
[18] M. Shafaei-Fallah, A. Rothenberger, A. P. Katsoulidis, J. He, C. D. Malliakas, M. G. Kanatzidis, *Adv. Mater.* **2011**, *23*, 4857.
[19] M. J. Manos, M. G. Kanatzidis, *Chem. Sci.* **2016**, *7*, 4804.
[20] S. M. Islam, K. S. Subrahmanyam, C. D. Malliakas, M. G. Kanatzidis, *Chem. Mater.* **2014**, *26*, 5151.
[21] S. Sidhik, Y. Wang, M. De Siena, R. Asadpour, A. J. Torma, T. Terlier, K. Ho, W. Li, A. B. Puthirath, X. Shuai, A. Agrawal, B. Traore, M. Jones, R. Giridharagopal, P. M. Ajayan, J. Strzalka, D. S. Ginger, C. Katan, M. A. Alam, J. Even, M. G. Kanatzidis, A. D. Mohite, *Science* **2022**, *377*, 1425.

[22] E. Ahmed, A. Rothenberger, *Microporous Mesoporous Mater.* **2014**, *199*, 74.
[23] M. Shafaei-Fallah, J. He, A. Rothenberger, M. G. Kanatzidis, *J. Am. Chem. Soc.* **2011**, *133*, 1200.
[24] K. Polychronopoulou, C. D. Malliakas, J. He, M. G. Kanatzidis, *Chem. Mater.* **2012**, *24*, 3380.
[25] A. Blanton, T. Islam, S. C. Roy, A. Celik, J. Nie, D. R. Baker, D. Li, K. Taylor-Pashow, X. Zhu, A. Pramanik, R. Amin, R. Feng, R. Chernikov, S. M. Islam, *Chem. Mater.* **2023**, *35*, 10446.
[26] L. Yang, L. Xie, M. Chu, H. Wang, M. Yuan, Z. Yu, C. Wang, H. Yao, S. M. Islam, K. Shi, D. Yan, S. Ma, M. G. Kanatzidis, *Angew Chem Int Ed Engl* **2022**, *61*, 202112511.
[27] L. Ma, Q. Wang, S. M. Islam, Y. Liu, S. Ma, M. G. Kanatzidis, *J. Am. Chem. Soc.* **2016**, *138*, 2858.
[28] R. G. Pearson, *J. Am. Chem. Soc.* **1963**, *85*, 3533.
[29] J. A. McCleverty, T. J. Meyer, J. E. Penner-Hahn, *Comprehensive Coordination Chemistry II: From Biology to Nanotechnology*, Elsevier Ltd, Amsterdam, Netherlands **2003**.
[30] D. P. Shoemaker, D. Y. Chung, J. F. Mitchell, T. H. Bray, L. Soderholm, P. J. Chupas, M. G. Kanatzidis, *J. Am. Chem. Soc.* **2012**, *134*, 9456.
[31] A. Mueller, W. O. Nolte, B. Krebs, *Inorg. Chem.* **1980**, *19*, 2835.
[32] S. M. Islam, J. D. Cain, F. Shi, Y. He, L. Peng, A. Banerjee, K. S. Subrahmanyam, Y. Li, S. Ma, V. P. Dravid, M. Grayson, M. G. Kanatzidis, *Chem. Mater.* **2018**, *30*, 3847.
[33] S. J. L. Billinge, M. G. Kanatzidis, *Chem. Commun.* **2004**, 749.
[34] S. M. Islam, J. Im, A. J. Freeman, M. G. Kanatzidis, *Inorg. Chem.* **2014**, *53*, 4698.
[35] Q. Gao, Z. Shi, K. Xue, Z. Ye, Z. Hong, X. Yu, M. Zhi, *Nanotechnology* **2018**, *29*, 215601.
[36] D. Sarma, C. D. Malliakas, K. S. Subrahmanyam, S. M. Islam, M. G. Kanatzidis, *Chem. Sci.* **2016**, *7*, 1121.
[37] S. M. Islam, S. Vanishri, H. Li, C. C. Stoumpos, J. A. Peters, M. Sebastian, Z. Liu, S. Wang, A. S. Haynes, J. Im, A. J. Freeman, B. Wessels, M. G. Kanatzidis, *Chem. Mater.* **2015**, *27*, 370.
[38] L. Ma, S. M. Islam, H. Liu, J. Zhao, G. Sun, H. Li, S. Ma, M. G. Kanatzidis, *Chem. Mater.* **2017**, *29*, 3274.
[39] C. Bresson, S. Esnouf, C. Lamouroux, P. L. Solari, C. D. Auwer, *New J. Chem.* **2006**, *30*, 416.
[40] S. E. Shadle, J. E. Penner-Hahn, H. J. Schugar, B. Hedman, K. O. Hodgson, E. I. Solomon, *J. Am. Chem. Soc.* **1993**, *115*, 767.
[41] M. Newville, *J. Phys.: Conf. Ser.* **2013**, *430*, 012007.
[42] M. Newville, *J. Synchrotron Radiat.* **2001**, *8*, 96.
[43] R. W. G. Wyckoff, *Crystal Structures*, 2nd ed. (Eds.: R. W. G. Wyckoff), Interscience Publishers, New York, **1963**.
[44] D. M. Pasquariello, R. Kershaw, J. D. Passaretti, K. Dwight, A. Wold, *Inorg. Chem.* **1984**, *23*, 872.
[45] P. Vaqueiro, M. L. Kosidowski, A. V. Powell, *Chem. Mater.* **2002**, *14*, 1201.
[46] T. Islam, M. Li, A. Blanton, K. A. Pitton, K. R. Rao, S. Bayat, K. M. Wiaderek, M. A. Weret, S. C. Roy, R. Feng, D. Li, R. Alam, J. Nie, O. Oketola, A. Pramanik, B. S. Guiton, C. Risko, I. Belharouak, R. Amin, S. M. Islam, *ACS Energy Lett.* **2024**, *9*, 1.
[47] L. Chen, S. Feng, D. Zhao, S. Chen, F. Li, C. Chen, *J. Colloid Interface Sci.* **2017**, *490*, 197.
[48] Y. Liu, C. Fang, S. Zhang, W. Zhong, Q. Wei, Y. Wang, Y. Dai, Y. Wang, Z. Zhang, Y. Liu, *Surfaces and Interfaces* **2020**, *18*, 100409.
[49] J. Wang, S. Yang, G. Cheng, P. Gu, *J. Chem. Eng. Data* **2020**, *65*, 2178.
[50] M. J. Manos, M. G. Kanatzidis, *J. Am. Chem. Soc.* **2012**, *134*, 16441.
[51] A. A. Sharfalddin, A.-H. Emwas, M. Jaremko, M. A. Hussien, *PLoS One* **2021**, *16*, 0256186.
[52] B. J. Riley, J. Chun, W. Um, W. C. Lepry, J. Matyas, M. J. Olszta, X. Li, K. Polychronopoulou, M. G. Kanatzidis, *Environ. Sci. Technol.* **2013**, *47*, 7540.

